MULTIBODY DYNAMICS 2009, ECCOMAS Thematic Conference
K. Arczewski, J. Frączek, M. Wojtyra (eds.)
Warsaw, Poland, 29 June – 2 July 2009

MULTIBODY MODELING OF RAILWAY VEHICLES: AN INNOVATIVE ELASTIC WHEEL – RAIL CONTACT MODEL

Silvia Magheri*, Monica Malvezzi*, Enrico Meli*, Andrea Rindi*

* Department of Energy Engineering S. Stecco
University of Florence, Via S. Marta 3, 50139, Florence, Italy
e-mail: silvia.magheri@unifi.it, malvezzi@mapp1.de.unifi.it, meli@mapp1.de.unifi.it, rindi@mapp1.de.unifi.it
web page: `http://mapp1.de.unifi.it`

Keywords: Multibody modeling, wheel – rail contact, contact between elastic bodies.

Abstract. *The wheel – rail contact analysis plays a fundamental role in the multibody modeling of railway vehicles. A good contact model must provide an accurate description of the global and local contact phenomena (contact forces, position and shape of the contact patch, stress and strain) and a general handling of the multiple contact. The model has also to assure high numerical efficiency and a good compatibility with commercial multibody software (Simpack Rail, Adams Rail).*

In this work the authors intend to present an innovative elastic wheel – rail contact model that satisfies the previous specifics. The model considers the wheel and the rail as elastic deformable bodies and requires the numerical solution of the Navier's elasticity equation. The contact between wheel and rail has been described by means of suitable analytical contact conditions. Subsequently the contact model has been inserted within the multibody model of a benchmark railway vehicle (the Manchester Wagon) in order to obtain a complete model of the wagon. The whole model has been implemented in the Matlab/Simulink environment. Finally numerical simulations of the vehicle dynamics have been carried out on many different railway tracks with the aim of evaluating the performances of the model.

The multibody model of the same vehicle (this time equipped with a standard contact model) has been then implemented also in Simpack Rail. The comparison between the results obtained by the Matlab model and those obtained by the Simpack model has allowed an accurate and reliable validation of the new contact model.

In conclusion the main purpose of the authors is to achieve a better integration between the differential modeling and the multibody modeling. This kind of integration is almost absent in literature (especially in the railway field) due to the computational cost and to the memory consumption. However it is very important because only the differential modeling allows an accurate analysis of the contact problem (in terms of contact forces, position and shape of the contact patch, stress and strain) while the multibody modeling is currently the standard in the study of the railway dynamics.

1 INTRODUCTION

The multibody simulation of the railway vehicle dynamics needs a reliable contact model that satisfies the following specifics: accurate description of the global and local contact phenomena (contact forces, position and shape of the contact patch, stress and strain), general and robust handling of the multiple contact, high numerical efficiency and compatibility with commercial multibody software (Simpack Rail, Adams Rail).

The wheel – rail contact problem has been discussed by several authors and many models can be found in the literature. Currently the main multibody approaches to the problem are the so - called rigid contact formulation and the semi - elastic contact description. The rigid approach considers the wheel and the rail as rigid bodies. The contact is imposed by means of constraint equations and the contact points are detected during the dynamic simulation by solving the nonlinear algebraic differential equations associated to the constrained multibody system. Indentation between the bodies is not permitted and the normal contact forces are calculated through the Lagrange multipliers. Finally the Hertz's and the Kalker's theories allow to evaluate respectively the shape of the contact patch and the tangential forces. [1] [2] [3] [4] [5] [6] Also the semi – elastic approach considers the wheel and the rail as rigid bodies. However in this case there are not constraints and the indentation between the bodies is permitted. The contact points are detected by means of approximated procedures (based on look – up tables and simplifying hypotheses on the problem geometry) or by means of semi – analytical methods (based on the reduction of the problem dimension). The normal contact forces are calculated as a function of the indentation while, as in the rigid approach, the Hertz's and the Kalker's theories allow to evaluate the shape of the contact patch and the tangential forces. [4] [5] [6] [7] [8] [9] Both the described multibody approaches are computationally very efficient but their generality and accuracy turn out to be often insufficient because the physical hypotheses behind these theories are too restrictive and, in many circumstances, unverified.

In order to obtain a complete description of the contact phenomena, differential contact models are needed. In other words wheel and rail have to be considered elastic bodies governed by the Navier's equations and the contact has to be described by suitable analytical contact conditions. The contact between elastic bodies has been widely studied in literature both in the general case and in the rolling case. Many procedures based on variational inequalities, FEM techniques and convex optimization have been developed. This kind of approach assures high generality and accuracy but still needs very large computational costs and memory consumption. [4] [10] [11] [12] [13] [14] [15] Due to the high computational load, referring to the current state of the art, the integration between multibody and differential modeling is almost absent in literature especially in the railway field. However this integration is very important because only the differential modeling allows an accurate analysis of the contact problem (in terms of contact forces, position and shape of the contact patch, stress and strain) while the multibody modeling is the standard in the study of the railway dynamics.

In this work the authors intend to present an innovative differential contact model with the aim of achieving a better integration between multibody and differential modeling. The new contact model is fully 3D and satisfies all the specifics described above. The developed procedure requires the discretization of the elastic contact problem (Navier's equations and analytical contact condition) and subsequently the solution of the nonlinear discrete problem. Both the steps have been implemented in Matlab/Simulink environment. At this point the contact model has been inserted within a 2D multibody model of a railway vehicle to obtain a complete model of the wagon. The railway vehicle chosen as benchmark is the Manchester

Wagon the physical and geometrical characteristics of which are easily available in the literature. [16] The choice of a 2D multibody model allows to study the lateral vehicle dynamics and at the same time to reduce the computational load. In the near future fully 3D multibody models will be considered in order to have a complete description of the vehicle dynamics. The multibody model has been implemented in SimMechanics, a Matlab toolbox specifically designed for multibody dynamics. The 2D multibody model of the same vehicle (this time equipped with a standard contact model based on the semi – elastic approach) has been then implemented also in Simpack Rail, a commercial multibody software for railway vehicles widely tested and validated. Finally numerical simulations of the vehicle dynamics have been carried out on many different railway tracks with the aim of evaluating the performances of the whole model. The comparison between the results obtained by the Matlab model and those obtained by the Simpack Rail model has allowed an accurate and reliable validation of the new contact model.

2 GENERAL ARCHITECTURE OF THE MODEL

As said in the introduction the whole model consists of two different part: the 2D multibody model of the railway vehicle and the fully 3D differential wheel – rail contact model. The 2D model has been obtained from a fully 3D multibody model of the benchmark vehicle (the Manchester Wagon) in order to simulate the lateral dynamics of the wagon and to reduce the computational load (Fig. (1)). The 2D model consists of three bodies: a car – body, a bogie and a wheelset. The car - body and the bogie have 3 DOFs (lateral and vertical displacement and roll) while the wheelset has 4 DOFs (lateral and vertical displacement, roll and pitch, i.e. the rotation around its symmetry axis). In other words the wheelset has been considered as a 3D body.

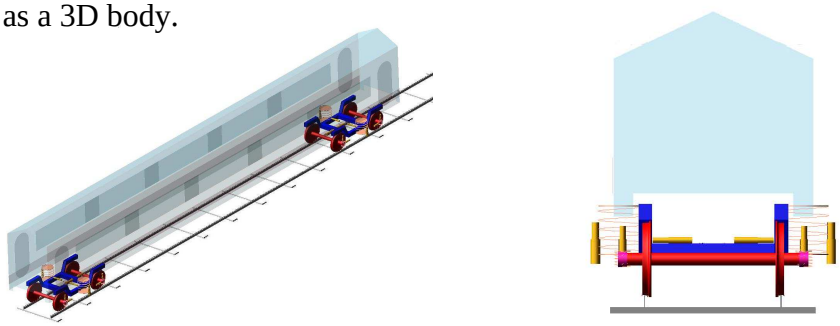

Figure 1: 3D and 2D multibody models of the Manchester Wagon (Matlab/Simulink).

During the simulation the 2D multibody model interacts with the fully 3D differential contact model. The general architecture of the model is schematically shown in Fig. (2).

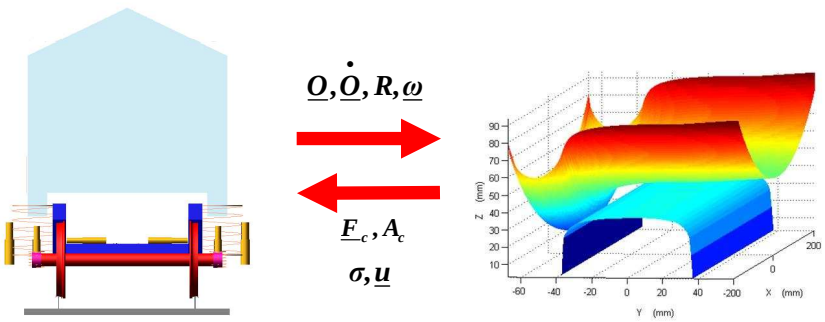

Figure 2: General architecture of the model.

At each integration step the multibody model evaluates the kinematic variables relative to the wheelset and consequently to each wheel – rail pair. Starting from these quantities, the contact model, based on Navier's equations and suitable contact conditions, calculates the global and local contact variables (force, contact patch, stress and displacement). Finally the knowledge of the contact variables allows the multibody model to carry on the simulation of the vehicle dynamics.

3 REFERENCE SYSTEMS

The railway track can be considered as a 3D curve $\underline{\gamma}(s)$ expressed in a fixed reference system $O_f x_f y_f z_f$ (s is the curvilinear abscissa of $\underline{\gamma}$). Usually in the cartographic description of the track only the curvature $K(s)$ of $\underline{\gamma}(s)$, the track slope $p(s)$ and the cant $\beta(s)$ are known; however the knowledge of these parameters is enough to rebuild the curve $\underline{\gamma}(s)$. [9] [17]

In this work the lateral vehicle dynamics will be described in a local reference system $O_R x_R y_R z_R$ having the x_R axis tangent to the track in the point $O_R = \underline{\gamma}(s)$ and the z_R axis normal to the plane of the rails. In the considered case the time histories of the curvilinear abscissa $s(t)$ and of the origin $O_R = \underline{\gamma}(s(t))$ are supposed to be known (for instance they can be calculated by simulating independently the longitudinal vehicle dynamics).

The local system follows the motion of the whole model along the track so that the centers of mass of the bodies lie always on the plane $y_R z_R$. According to chapter 2, the car – body and the bogie can only translate along y_R and z_R and rotate around x_R while the wheelset can also rotate around its symmetry axis.

Subsequently a third reference system $O_W x_W y_W z_W$ is defined. The origin O_W coincides with the center of mass of the wheelset and the y_W axis with its symmetry axis. This system is fixed to the wheelset except for the rotation around the y_W axis. Finally two reference systems $O_b x_b y_b z_b$ and $O_B x_B y_B z_B$ are introduced, fixed respectively to the bogie and to the car - body. As usual the origins coincide with the centers of mass. The placement of the reference systems is illustrated in Fig. (3).

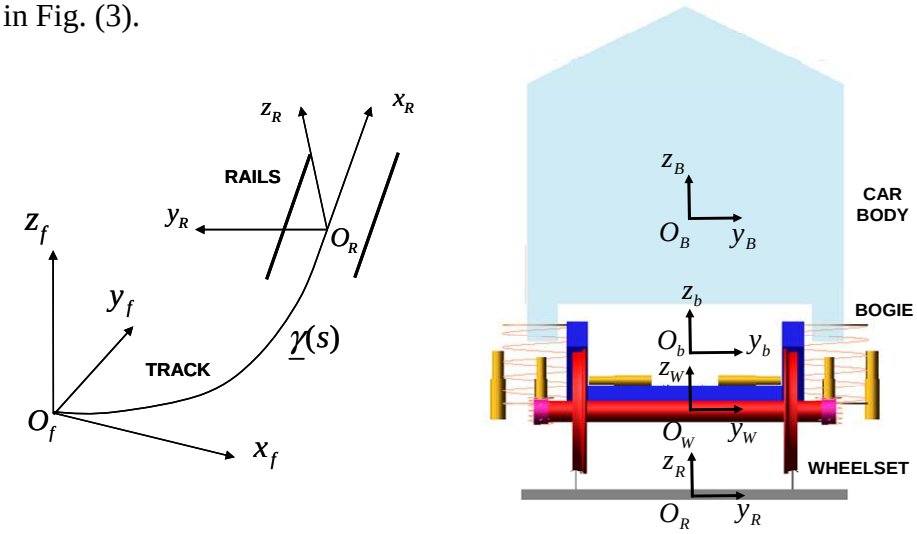

Figure 3: Reference systems relative to the multibody model.

In order to correctly describe the differential contact model, two further reference systems have to be defined for each wheel – rail pair. For the sake of simplicity only the left pair has

been reported in Fig. (4). The first system $O_{lw}x_{lw}y_{lw}z_{lw}$ is parallel to the system $O_W x_W y_W z_W$ and its origin O_{lw} lies on the symmetry axis of the wheel. The system is fixed to the wheel except for the rotation around the y_{lw} axis. Moreover the origin O_{lw} belongs to the nominal rolling plane, i. e. the plane normal to the rotation axis containing the nominal rolling radius. The second system $O_{lr}x_{lr}y_{lr}z_{lr}$ is parallel to the system $O_R x_R y_R z_R$. Its origin O_{lr} belongs to the axis y_R while the distance between O_R and O_{lr} has to assure the correct gauge between the rails. Both the reference systems described above are very important because the global and local contact variables will be evaluated by the contact model just in these systems.

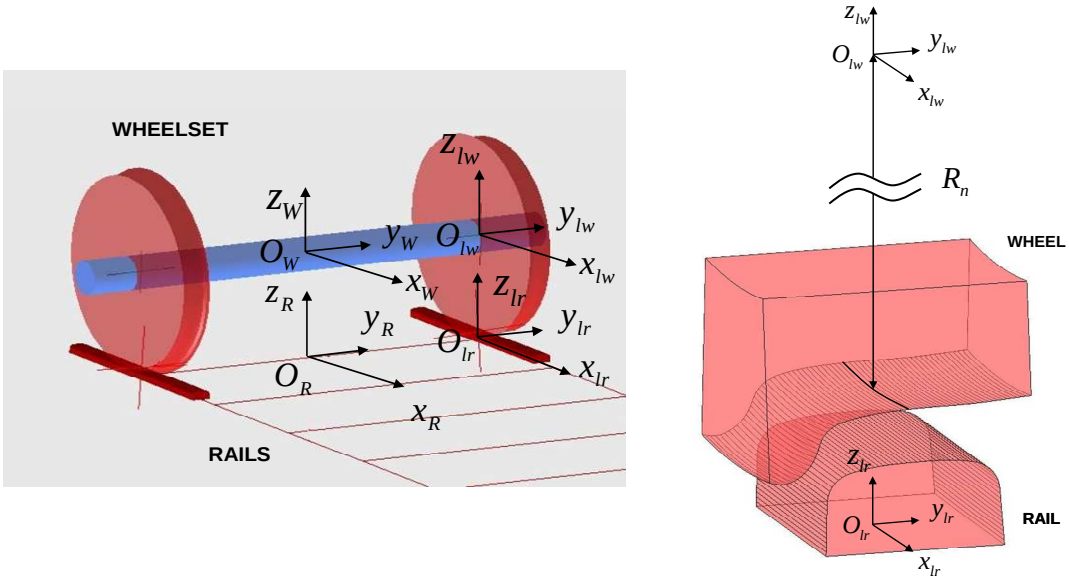

Figure 4: Reference systems relative to the differential contact model.

Finally, as regards the external forces acting on the bodies, some considerations are needed. As said before, the lateral vehicle dynamics is studied in the local reference system $O_R x_R y_R z_R$ but this system is not inertial. Therefore the multibody model will have to consider the effect of the fictitious forces (centrifugal force and Coriolis force). These quantities can be calculated starting from the knowledge of the kinematics of the bodies as a function of the curvature $K(s)$, the track slope $p(s)$ and the cant $\beta(s)$. [17]

4 THE 2D MULTIBODY MODEL

The 2D multibody model has been obtained from a fully 3D multibody model of the Manchester Wagon, the physical and geometrical characteristics of which are easily available in the literature. [16] The original 3D model consists of:
- 1 car – body, 2 bogies and 4 wheelsets
- rear and front primary suspensions
- rear and front secondary suspensions (including roll bar, traction rod and bumpstop).

Both the primary and the secondary suspensions are usually modeled by means of nonlinear force elements like three- dimensional springs and dampers. The 2D model can be thought of as a section of the 3D model and comprises (Fig. (5)):
- one car – body, one bogie and one wheelset
- one primary suspension
- one secondary suspension (including roll bar and bumpstop).

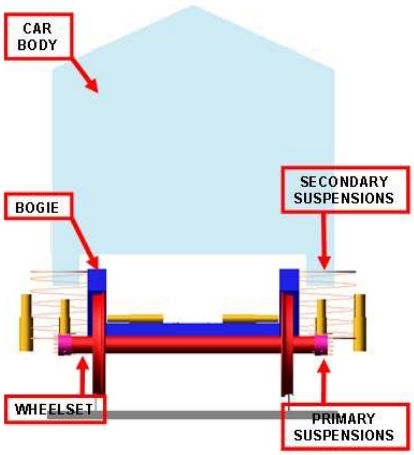

Figure 5: 2D multibody model of the Manchester Wagon.

Body	Mass	Inertia
Car – body	0.25	0.25
Bogie	0.5	0.5
Wheelset	1	1

Table 1: Scaling factors (mass and inertia).

Suspensions	Springs	Dampers
Secondary	0.5	0.5
Primary	1	1

Table 2: Scaling factors (springs and dampers).

As regards the bodies, only some DOFs are allowed by the 2D model:
- the car – body and the bogie have 3 DOFs; they can translate along the axes y_R and z_R (lateral and vertical displacements) and rotate around the x_R axis (roll)
- the wheelset, considered as a 3D body, has 4 DOFs; besides the previous DOFs it can also rotate around its symmetry axis y_W (pitch).

Moreover, in order to assure the dynamic equivalence between the 2D model and the original 3D model, the inertial characteristics of the bodies and the physical characteristics of the force elements have to be correctly scaled down. [5] [16] The values of the scaling factors are schematically reported in Tab. (1) and Tab. (2).

The choice of a 2D multibody model has been made with the aim of studying the lateral vehicle dynamics and, at the same time, of reducing the computational load. In the near future fully 3D multibody models of the Manchester Wagon will be considered in order to have a complete description of the vehicle dynamics.

5 THE 3D DIFFERENTIAL CONTACT MODEL

As regards the generic contact variable Z, the following convention will be adopted:
- Z_w and Z_w^r will denote a variable relative to the wheel respectively expressed in the reference systems $O_{lw}x_{lw}y_{lw}z_{lw}$ and $O_{lr}x_{lr}y_{lr}z_{lr}$
- Z_r and Z_r^w will denote a variable relative to the rail respectively expressed in the reference systems $O_{lr}x_{lr}y_{lr}z_{lr}$ and $O_{lw}x_{lw}y_{lw}z_{lw}$.

In the future, according to this convention, the various changes of reference system won't be continually remarked but will be taken for granted.

5.1 Inputs and Outputs

With reference to Fig. (2), the contact model can be thought of as a black box having the following inputs and outputs:
- INPUTS: the kinematic variables relative to the considered wheel – rail pair (in this case the left one), i.e. the position $\underline{O}_w^r$, the velocity $\dot{\underline{O}}_w^r$, the orientation R_w^r and the angular velocity $\underline{\omega}_w^r$ of the reference system $O_{lw}x_{lw}y_{lw}z_{lw}$ with respect to the system $O_{lr}x_{lr}y_{lr}z_{lr}$ (see Fig. (4)).
- OUTPUTS: the global and local contact variables relative to the wheel and to the rail, like

the contact forces $\underline{F}_{wC}$ and $\underline{F}_{rC}$, the stresses σ_w and σ_r, the displacements $\underline{u}_w$ and $\underline{u}_r$ and the contact patches A_{wC} and A_{rC}.

5.2 The kinematics of the problem

The wheel and the rail have been considered as two linear elastic bodies Ω_w and Ω_r (as shown in Fig. (6)). Both the domains are supposed to be sufficiently large compared to the dimensions of the contact patch. [12] [13]

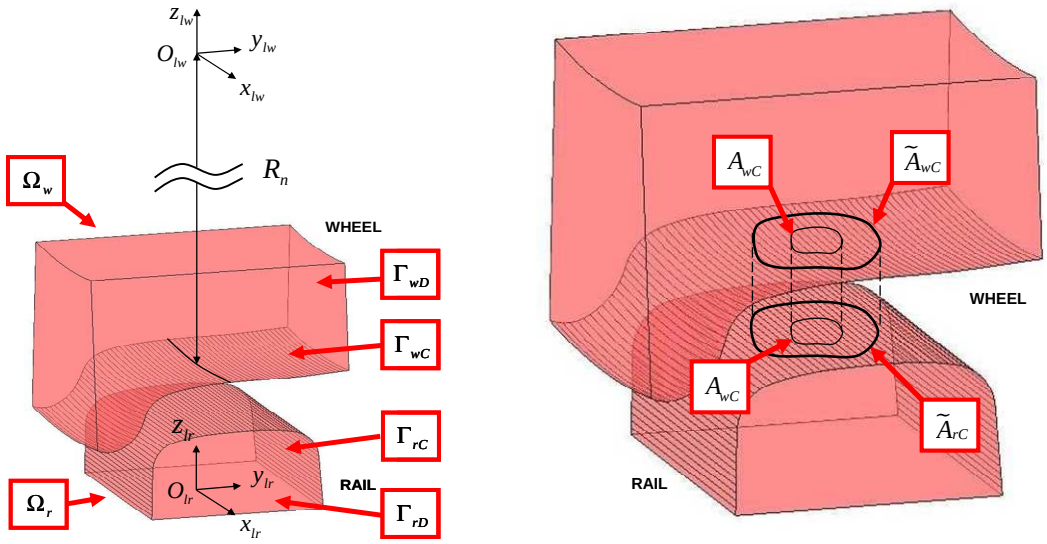

Figure 6: The problem geometry.

The boundaries $\partial\Omega_w$ and $\partial\Omega_r$ are split into two disjoint regions, respectively Γ_{wD}, Γ_{wC} and Γ_{rD}, Γ_{rC}. Within the regions Γ_{wD} and Γ_{rD} the displacements are fixed (and equal to zero) while Γ_{wC} and Γ_{rC} (dashed in the figure) are the regions where the contact may occur.

In case of contact the geometric intersection between the surfaces Γ_{wC} and Γ_{rC} (and thus between the non – deformed configurations) allows to define two regions $\tilde{A}_{wC} \subset \Gamma_{wC}$ and $\tilde{A}_{rC} \subset \Gamma_{rC}$ (with $\tilde{A}_{wC} \simeq \tilde{A}_{rC}$) that can be considered as a rough estimate of the contact areas. The situation is schematically sketched in Fig. (6) and Fig. (7).

The real contact areas $A_{wC} \subset \tilde{A}_{wC}$ and $A_{rC} \subset \tilde{A}_{rC}$ (with $A_{wC} \simeq A_{rC}$) are unknown and have to be calculated by the model. For this purpose a contact map $\underline{\Phi}$ has to be introduced. The contact map $\underline{\Phi} : \tilde{A}_{wC} \rightarrow \tilde{A}_{rC}$ (by convention the wheel is the master body) locates the position of the point $\underline{\Phi}(\underline{x}_w^r) \in \tilde{A}_{rC}$ that will come in contact with the generic point $\underline{x}_w^r \in \tilde{A}_{wC}$. In this case the map $\underline{\Phi}$ is defined as the normal projection $\underline{\Phi}(\underline{x}_w^r)$ of the point $\underline{x}_w^r \in \tilde{A}_{wC}$ on the surface $\tilde{A}_{rC}$. Starting from the contact map, the distance function between the deformed configurations $d : \tilde{A}_{wC} \rightarrow R$ can be evaluated:

$$d(\underline{x}_w^r) = \left(\underline{u}_w^r - \underline{u}_r\right) \bullet \underline{n}_w^r - \left(\underline{\Phi}(\underline{x}_w^r) - \underline{x}_w^r\right) \bullet \underline{n}_w^r \qquad (1)$$

where $\underline{n}_w^r$ is the outgoing normal versor to the surfaces Γ_{wC}. The function d is positive if there is penetration between the deformed configurations and negative otherwise.

Formally the contact area A_{wC} is defined as the region of $\tilde{A}_{wC}$ where the function d is positive while the contact area $A_{rC} = \underline{\Phi}(A_{wC})$ is the normal projection of A_{wC} on $\tilde{A}_{rC}$. In other words, from a kinematic point of view, the penetration between the deformed bodies is allowed and will play a fundamental role in the contact model (see paragraph 5.3). [12][13]

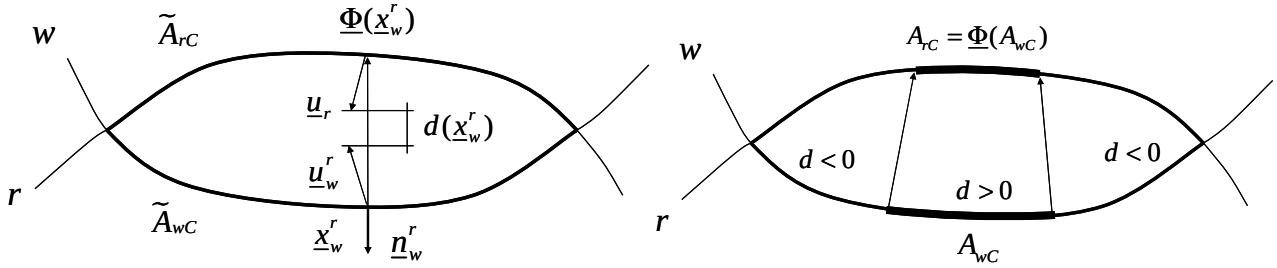

Figure 7: Contact map and distance function.

In this way the estimated contact areas $\tilde{A}_{wC}$ and $\tilde{A}_{rC}$ depend only on the relative wheel – rail kinematics ($\underline{O}_w^r$, $\dot{\underline{O}}_w^r$, R_w^r and $\underline{\omega}_w^r$) while the real contact areas A_{wC} and A_{rC} depend also on the displacements $\underline{u}_w$ and $\underline{u}_r$. Finally it is useful to remark that no hypothesis has been made on the shape of the contact patch; in particular, the contact patch can be formed of one or more disjoint parts.

As regards the wheel and rail profiles, the standard ORE S 1002 and UIC 60 have been used. [17]

5.3 The contact model

According to the linear theory of elasticity [12] [13], both the wheel and the rail are governed by the Navier's equations:

$$\begin{aligned} &div\ \sigma_w(\underline{u}_w) = \underline{0} \text{ on } \Omega_w \qquad && \sigma_w(\underline{u}_w)\underline{n}_w = \underline{p}_w \text{ on } \tilde{\Gamma}_{wC} \\ &div\ \sigma_r(\underline{u}_r) = \underline{0} \text{ on } \Omega_r && \sigma_w(\underline{u}_w)\underline{n}_w = \underline{0} \text{ on } \Gamma_{wC} \setminus \tilde{\Gamma}_{wC} \\ &\underline{u}_w = \underline{0} \text{ on } \Gamma_{wD} && \sigma_r(\underline{u}_r)\underline{n}_r = \underline{p}_r \text{ on } \tilde{\Gamma}_{rC} \\ &\underline{u}_r = \underline{0} \text{ on } \Gamma_{rD} && \sigma_r(\underline{u}_r)\underline{n}_r = \underline{0} \text{ on } \Gamma_{rC} \setminus \tilde{\Gamma}_{rC} \end{aligned} \tag{2}$$

where $\underline{n}_w$ and $\underline{n}_r$ are the outgoing normal vectors to the surfaces Γ_{wC} and Γ_{rC} while $\underline{p}_w$ and $\underline{p}_r$ are the unknown contact pressures. The pressures $\underline{p}_w$ and $\underline{p}_r$ are defined on $\tilde{A}_{wC}$ and $\tilde{A}_{rC}$ but, according to paragraph 5.2, will have to be zero on $\tilde{A}_{wC} \setminus A_{wC}$ and $\tilde{A}_{rC} \setminus A_{rC}$. Both the bodies have the material characteristics of the steel (Young's modulus $E_w = E_r = 2.1*10^{11}\,Pa$ and Poisson's coefficient $\nu_w = \nu_r = 0.3$).

In the studied case the volume forces (i. e. the gravity) have been neglected because the multibody model of the wheelset already considers their effect. Moreover, since the solution is supposed to be steady within the integration step (see Fig. (2)), also the inertial terms have been omitted.

Equivalently the problem (2) can be formulated in weak form as follows:

$$\begin{aligned} \int_{\Omega_w} \sigma_w(\underline{u}_w) : \varepsilon_w(\underline{v}_w) dV &= \int_{\widetilde{A}_{wC}} \underline{p}_w \bullet \underline{v}_w dA \quad \forall \underline{v}_w \in V_w \\ \int_{\Omega_r} \sigma_r(\underline{u}_r) : \varepsilon_r(\underline{v}_r) dV &= \int_{\widetilde{A}_{rC}} \underline{p}_r \bullet \underline{v}_r dA \quad \forall \underline{v}_r \in V_r \end{aligned} \tag{3}$$

where ε_w and ε_r are the strains while V_w and V_r are suitable Sobolev's spaces.

In order to complete the contact model, the contact pressures $\underline{p}_w$ and $\underline{p}_r$ have to be expressed as a function of the displacements $\underline{u}_w$ and $\underline{u}_r$. For the sake of simplicity the normal and the tangential contact pressures on the wheel are introduced: $p^r_{wN} = \underline{p}^r_w \bullet \underline{n}^r_w$, $\underline{p}^r_{wT} = \underline{p}^r_w - p^r_{wN}\underline{n}^r_w$. The normal pressure p^r_{wN} has been calculated by means of the distance function d:

$$p^r_{wN}(\underline{x}^r_w) = -K \max(d(\underline{x}^r_w), 0) \quad \text{on } \widetilde{A}_{wC} \tag{4}$$

where $K > 0$ is a fictitious stiffness constant. The value of K have to be chosen large enough to assure the accuracy required by this kind of problems. The condition of ideal contact (total absence of penetration between the deformed bodies) is reached for $K \to +\infty$ (usually $K \geq 10 \wedge 15$ N/m^3).[12][13]

To evaluate the tangential pressure $\underline{p}^r_{wT}$, the slip $\underline{s}^r_w$ between the wheel and rail surfaces has to be defined. Since the solution is supposed to be steady within the integration step, the following expression holds: [4]

$$\begin{aligned} \underline{s}^r_w(\underline{x}^r_w) &= \underline{w}^r_w(\underline{x}^r_w) + \dot{\underline{u}}^r_w(\underline{x}^r_w) - \underline{w}_r(\Phi(\underline{x}^r_w)) - \dot{\underline{u}}_r(\Phi(\underline{x}^r_w)) = \\ &= \underline{w}^r_w(\underline{x}^r_w) + J^r_w(\underline{x}^r_w)\underline{w}^r_w(\underline{x}^r_w) - \underline{w}_r(\Phi(\underline{x}^r_w)) - J_r(\Phi(\underline{x}^r_w))\underline{w}_r(\Phi(\underline{x}^r_w)) \end{aligned} \tag{5}$$

where $\underline{w}^r_w$ and $\underline{w}_r$ are the rigid velocity of the points $\underline{x}^r_w$ and $\Phi(\underline{x}^r_w)$ while J^r_w and J_r are the Jacobians of $\underline{u}^r_w$ and $\underline{u}_r$. As usual the normal and the tangential slips are: $s^r_{wN} = \underline{s}^r_w \bullet \underline{n}^r_w$, $\underline{s}^r_{wT} = \underline{s}^r_w - s^r_{wN}\underline{n}^r_w$. According to the standard friction models, the tangential pressures $\underline{p}^r_{wT}$ can be expressed as follows:

$$\underline{p}^r_{wT}(\underline{x}^r_w) = \begin{cases} \underline{0} & \text{if } s^r_{wT}(\underline{x}^r_w) = 0 \\ -\mu(s^r_{wT}(\underline{x}^r_w), V)\left|p^r_{wN}(\underline{x}^r_w)\right| \dfrac{\underline{s}^r_{wT}(\underline{x}^r_w)}{s^r_{wT}(\underline{x}^r_w)} & \text{if } s^r_{wT}(\underline{x}^r_w) > 0 \end{cases} \quad \text{on } \widetilde{A}_{wC} \tag{6}$$

where s^r_{wT} is the norm of $\underline{s}^r_{wT}$ and V is the longitudinal velocity of the vehicle. Further details on the friction function $\mu(s^r_{wT}, V)$ can be found in the literature. [19]

Finally the action – reaction principle (the Newton's Third Law) allows to calculate the pressures $\underline{p}_r$:

$$\underline{p}_r(\Phi(\underline{x}^r_w)) = -\underline{p}^r_w(\underline{x}^r_w) \quad \text{on } \widetilde{A}_{wC}. \tag{7}$$

It is useful to remark that, according to the described model, the pressures $\underline{p}^r_w$ and $\underline{p}_r$ are zero respectively on $\widetilde{A}_{wC} \setminus A_{wC}$ and $\widetilde{A}_{rC} \setminus A_{rC}$.

The displacements $\underline{u}_w$ and $\underline{u}_r$ will be evaluated in the following through the numerical solution of Eq. (3). The knowledge of these unknown quantities will allow to calculate all the other required outputs like the contact areas A_{wC} and A_{rC} and the stresses σ_w and σ_r. The contact forces $\underline{F}_{wC}$ and $\underline{F}_{rC}$ will be estimated by integration:

$$\underline{F}_{wC} = \int_{\tilde{A}_{wC}} \underline{p}_w dA \quad \underline{F}_{rC} = \int_{\tilde{A}_{rC}} \underline{p}_r dA. \tag{8}$$

5.4 The discretization of the model

Both the elastic bodies have been discretized by means of tetrahedral elements and linear shape functions. The meshes have been built according to the standard Delaunay's algorithms (see Fig. (8)). [18]

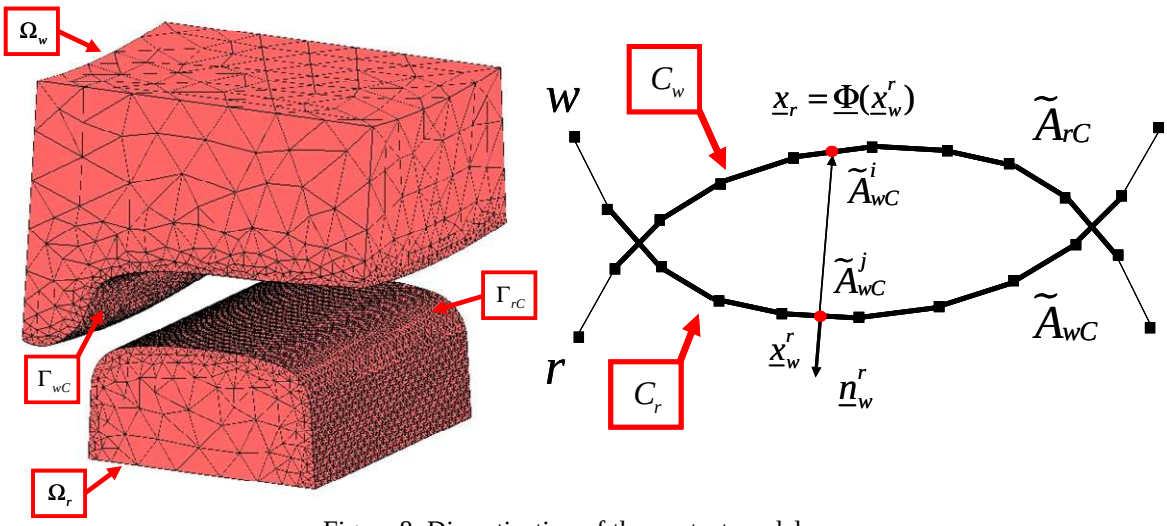

Figure 8: Discretization of the contact model.

The resolution of the meshes on the surfaces Γ_{wC} and Γ_{rC} is constant (usually in the range $1\text{mm} \div 2\text{mm}$) because the position and the dimensions of the contact patch are a priori unknown. The surface resolution has also to assure an accuracy enough to correctly describe the contact phenomena. Moreover it is important to remark that the meshes have been created directly in the reference systems $O_{lw}x_{lw}y_{lw}z_{lw}$ and $O_{lr}x_{lr}y_{lr}z_{lr}$; therefore they don't change during the simulation and can be easily built off – line.

In the future the following convention will be adopted:

- the sets of all the elements of wheel and rail will be called T_w and T_r while the vectors $\underline{u}_{w\,h}, \underline{u}_{r\,l} \in R^{12}$ will contain the displacements of the four nodes belonging to the elements $h \in T_w$ and $l \in T_r$. Finally the vectors $\underline{U}_w$ and $\underline{U}_r$ will comprise the displacements relative to all the nodes of wheel and rail. Since the displacements on Γ_{wD} and Γ_{rD} are zero, the dimension of $\underline{U}_w$, $\underline{U}_r$ are $3(N_w - N_{wD})$ and $3(N_r - N_{rD})$, where N_w and N_r are the numbers of nodes of wheel and rail while N_{wD} and N_{rD} are the numbers of nodes on Γ_{wD} and Γ_{rD}.
- similarly C_w and C_r will be the sets of the active contact elements on wheel and on rail, i. e. the sets of the elements having respectively a face $\tilde{A}_{wC}^i$ and $\tilde{A}_{rC}^j$ that lies on $\tilde{A}_{wC}$ and $\tilde{A}_{rC}$. The vectors $\underline{u}_{w\,i}, \underline{u}_{r\,j} \in R^{12}$ will contain the displacements of the four nodes belonging to the

elements $i \in C_w$ and $j \in C_r$ while the vectors $\underline{U}_{wC}$ and $\underline{U}_{rC}$ will comprise the displacements relative to all the active elements. The dimension of $\underline{U}_{wC}$, $\underline{U}_{rC}$ are $3N_{wC}$ and $3N_{rC}$ where N_{wC} and N_{rC} are the number of nodes belonging to the active elements.

The knowledge of the relative kinematics ($\underline{O}_w^r$, $\dot{\underline{O}}_w^r$, R_w^r and $\underline{\omega}_w^r$) and consequently of the estimated contact areas $\widetilde{A}_{wC}$ and $\widetilde{A}_{rC}$ allows to determine the sets C_w and C_r of the active contact elements on the wheel and on the rail.

For each active contact element on the wheel, the center $\underline{x}_{w\,i}^r$ of the face $\widetilde{A}_{wC}^i$ is considered. The normal projection $\underline{x}_{r\,j} = \underline{\Phi}(\underline{x}_{w\,i}^r)$ of $\underline{x}_{w\,i}^r$ on $\widetilde{A}_{rC}$ will belong to the external face $\widetilde{A}_{rC}^j$ of the j-th active contact element on the rail. In particular the index $j(i)$ will be a function of the index i. In other words the pairs of points ($\underline{x}_{w\,i}^r$, $\underline{x}_{r\,j(i)}$) with $i \in C_w$ can be thought of as the discretization of the contact map $\underline{\Phi}$. The situation is schematically sketched in Fig. (8).

The values of the displacements $\underline{u}_w^r$, $\underline{u}_r$ and of their Jacobians J_w^r, J_r in the points $\underline{x}_{w\,i}^r$ and $\underline{x}_{r\,j}$ are evaluated through the shape functions. [12] [13] [18]

At this point the distance function $d_i = d(\underline{x}_{w\,i}^r)$ and the pressure $\underline{p}_{w\,i}^r = \underline{p}_w^r(\underline{x}_{w\,i}^r)$ on the face $\widetilde{A}_{wC}^i$ of the active element of the wheel can be calculated by means of Eq. (1), (4) and (6). Finally a discrete version of the action – reaction principle (the Newton's Third Law) is needed to evaluate the pressure $\underline{p}_{r\,j} = \underline{p}_r(\underline{x}_{r\,j})$ on the face $\widetilde{A}_{rC}^j$ of the active element of the rail:

$$|\widetilde{A}_{rC}^j|\,\underline{p}_{r\,j} = |\widetilde{A}_{wC}^i|\,\underline{p}_{w\,i}^r \tag{9}$$

where $|\widetilde{A}_{wC}^i|$ and $|\widetilde{A}_{rC}^j|$ are the areas of the faces $\widetilde{A}_{wC}^i$ and $\widetilde{A}_{rC}^j$. Both the pressures $\underline{p}_{w\,i}^r$ and $\underline{p}_{r\,j}$ are supposed to be constant on $\widetilde{A}_{wC}^i$ and $\widetilde{A}_{rC}^j$.

The standard FEM techniques allow to discretize the weak form of the contact problem (see Eq. (3)) : [12] [13] [18]

$$\begin{aligned}
&\int_{\Omega_w} \sigma_w(\underline{u}_w) : \varepsilon_w(\underline{v}_w) dV = \sum_{h \in T_w} \underline{u}_{w\,h}^T K_{w\,h} \underline{v}_{w\,h} = \underline{U}_w^T K_w \underline{V}_w \qquad \int_{\widetilde{A}_{wC}} \underline{p}_w \bullet \underline{v}_w dA = \sum_{i \in C_w} \underline{p}_{w\,i}^T M_{w\,i} \underline{v}_{w\,i} = \underline{F}_w(\underline{U}_{wC}, \underline{U}_{rC})^T \underline{V}_w \\
&\int_{\Omega_r} \sigma_r(\underline{u}_r) : \varepsilon_r(\underline{v}_r) dV = \sum_{l \in T_r} \underline{u}_{r\,l}^T K_{r\,l} \underline{v}_{r\,l} = \underline{U}_r^T K_r \underline{V}_r \qquad \int_{\widetilde{A}_{rC}} \underline{p}_r \bullet \underline{v}_r dA = \sum_{j \in C_r} \underline{p}_{r\,j}^T M_{r\,j} \underline{v}_{r\,j} = \underline{F}_r(\underline{U}_{wC}, \underline{U}_{rC})^T \underline{V}_r
\end{aligned} \tag{10}$$

where $K_{w\,h}$, $K_{r\,l}$ are the stiffness matrices relative to the elements $h \in T_w$, $l \in T_r$ and $M_{w\,i}$, $M_{r\,j}$ depend on the shape functions. The global stiffness matrices K_w and K_r are symmetric, positive defined and sparse while the vectors $\underline{F}_w$ and $\underline{F}_r$, that contain the terms due to the contact pressures, are sparse. Moreover the global stiffness matrices are evaluated directly in the reference systems $O_{lw} x_{lw} y_{lw} z_{lw}$ and $O_{lr} x_{lr} y_{lr} z_{lr}$; therefore they don't change during the simulation and can be easily built off – line. Eq. (3) and Eq. (10), combined together, give

$$\begin{aligned}
&\underline{U}_w^T K_w \underline{V}_w = \underline{F}_w(\underline{U}_{wC}, \underline{U}_{rC})^T \underline{V}_w \quad \forall \underline{V}_w \in R^{3(N_w - N_{wD})} \\
&\underline{U}_r^T K_r \underline{V}_r = \underline{F}_r(\underline{U}_{wC}, \underline{U}_{rC})^T \underline{V}_r \quad \forall \underline{V}_r \in R^{3(N_r - N_{rD})}
\end{aligned} . \tag{11}$$

Finally, since the matrices K_w, K_r are symmetric and the vectors $\underline{V}_w$, $\underline{V}_r$ are arbitrary, the following nonlinear system of algebraic equations is obtained:

$$K_w \underline{U}_w = \underline{F}_w(\underline{U}_{wC}, \underline{U}_{rC}) \quad K_r \underline{U}_r = \underline{F}_r(\underline{U}_{wC}, \underline{U}_{rC}) \tag{12}$$

where, as said before, the contact displacements $\underline{U}_{wC}$, $\underline{U}_{rC}$ are a subset of the displacements $\underline{U}_w$, $\underline{U}_r$. Eq. (12) can be also written as

$$\underline{U}_w = H_w \underline{F}_w(\underline{U}_{wC}, \underline{U}_{rC}) \quad \underline{U}_r = H_w \underline{F}_r(\underline{U}_{wC}, \underline{U}_{rC}) \tag{13}$$

where the matrices $H_w = K_w^{-1}$ and $H_r = K_r^{-1}$ are symmetric, positive defined and full (consequently their storage can require an high memory consumption). Like K_w and K_r they don't change during the simulation and can be calculated off – line. Splitting $\underline{U}_w$, $\underline{U}_r$ into contact displacement $\underline{U}_{wC}$, $\underline{U}_{rC}$ and non – contact displacement $\underline{U}_{wNC}$, $\underline{U}_{wNC}$, Eq. (13) becomes

$$\begin{pmatrix} \underline{U}_{wNC} \\ \underline{U}_{wC} \end{pmatrix} = \begin{bmatrix} H_w^{11} & H_w^{12} \\ H_w^{21} & H_w^{22} \end{bmatrix} \begin{pmatrix} \underline{0} \\ \underline{f}_w(\underline{U}_{wC}, \underline{U}_{rC}) \end{pmatrix} \quad \begin{pmatrix} \underline{U}_{rNC} \\ \underline{U}_{rC} \end{pmatrix} = \begin{bmatrix} H_r^{11} & H_r^{12} \\ H_r^{21} & H_r^{22} \end{bmatrix} \begin{pmatrix} \underline{0} \\ \underline{f}_r(\underline{U}_{wC}, \underline{U}_{rC}) \end{pmatrix}. \tag{14}$$

In this way the second and the fourth components of Eq. (14) are sufficient to calculate contact displacement $\underline{U}_{wC}$, $\underline{U}_{rC}$:

$$\underline{U}_{wC} = H_w^{22} \underline{f}_w(\underline{U}_{wC}, \underline{U}_{rC}) \quad \underline{U}_{rC} = H_r^{22} \underline{f}_r(\underline{U}_{wC}, \underline{U}_{rC}). \tag{15}$$

The matrices H_w^{22} and H_r^{22} have the same properties as H_w and H_r but this time their dimensions are much smaller. However H_w^{22} and H_r^{22} change during the simulation and therefore have to be built directly on – line. The vectors $\underline{f}_w$ and $\underline{f}_r$ are full. The remaining non – contact displacements $\underline{U}_{wNC}$, $\underline{U}_{wNC}$ can be evaluated by means of the first and the third components of Eq. (14).

The knowledge of the displacements $\underline{U}_w$, $\underline{U}_r$, evaluated by solving Eq. (12) or Eq. (15), allows to calculate all the other required outputs like the contact areas A_{wC} and A_{rC} and the stresses σ_w and σ_r. The contact forces $\underline{F}_{wC}$ and $\underline{F}_{rC}$ are estimated by numerical integration:

$$\underline{F}_{wC} = \sum_{i \in C_w} |\, \widetilde{A}_{wC}^{i} \,|\, \underline{p}_{w\,i} \quad \underline{F}_{rC} = \sum_{j \in C_r} |\, \widetilde{A}_{rC}^{j} \,|\, \underline{p}_{r\,j}. \tag{16}$$

5.5 The numerical solution of the discrete problem

In this paragraph the numerical methods used for solving the discrete contact problem are presented. Both the formulations (12) and (15) will be analyzed in the following.

Eq. (12) is a large and sparse nonlinear system; on the contrary Eq. (15) is a full non linear system with much smaller dimensions than (12). The typical dimensions of K_w and K_r (depending on the mesh resolution) are in the range $10000 \div 50000$ while those of H_w^{22} and H_r^{22} (depending on the number of active elements) are about $100 \div 1000$.

Techniques based on Newton - Krylov methods are usually very efficient for solving large and sparse systems as Eq. (12). [20] Newton - Krylov methods are Newton-type methods for

the problem $\underline{F}(\underline{x})=\underline{0}$ where $\underline{F}$ is a generic nonlinear function. In particular, Krylov methods are employed to solve approximately the arising linear systems:

$$F'(\underline{x}_k)\underline{s}_k = -\underline{F}(\underline{x}_k) \tag{17}$$

where $F'(\underline{x})$ is the Jacobian matrix of $\underline{F}(\underline{x})$. The Krylov method computes, at each iteration, the so-called inexact Newton step $\tilde{\underline{s}}_k$ which satisfies the condition:

$$\left\| \underline{F}'(\underline{x}_k)\tilde{\underline{s}}_k + \underline{F}(\underline{x}_k) \right\| \le \eta_k \left\| \underline{F}(\underline{x}_k) \right\| \quad \eta_k \in [0,1) \tag{18}$$

where the forcing terms η_k are used to control the level of accuracy. [20] As regards the considered problem, numerical experimentations showed that, among all the Krylov methods, the best iterative linear solver is the BiCGStab. [21] This kind of numerical procedures are known as Newton - BiCGStab methods.

Iterative methods like the BiCGStab need often a good preconditioner. The employed preconditioner P has been defined as follows:

$$P = \begin{pmatrix} K_w & 0 \\ 0 & K_r \end{pmatrix}. \tag{19}$$

Since Eq. (12) is weakly nonlinear, the preconditioner P is a good approximation of the Jacobian matrix. In general, BiCGStab does not require the whole matrix P but only a factorization of it. In the considered case the incomplete Cholesky factorization [21] has been used because the matrix P is not only symmetric and positive defined but also sparse. In particular, this factorization performs a reordering of P and takes advantage of its sparsity in terms of execution time and memory consumption.

An interesting feature of Newton - BiCGStab methods is that they require only the action of $F'(\underline{x})$ on a vector $\underline{v}$ but not the computation and the storage of the whole Jacobian. In this case, the product $F'(\underline{x})v$ can be approximated by finite differences [22]:

$$F'(\underline{x})\underline{v} \simeq \frac{\underline{F}(\underline{x}+\varepsilon\underline{v}) - \underline{F}(\underline{x})}{\varepsilon} \tag{20}$$

where $\varepsilon > 0$ is a scalar small enough. Consequently these methods are called “matrix free”.

Moreover, it has to be remarked that, if the guarantee of convergence is only local, the numerical procedure may fail in finding a solution, even though an effective solution exists. Therefore the Newton-BiCGStab method has been embedded into a globalization strategy. A monotone line search method with Armijo rule has been employed, with a maximum of 10 backtracks for nonlinear iteration. [22] [23]

Finally it has been observed that a small number of nonlinear iterations is needed for solving the nonlinear system (12) and that the convergence is achieved in almost all cases. Consequently the choice of a less accurate solution of the Newton equations (17) turned out to be very efficient and effective in reducing the norm of $\underline{F}$. A constant forcing term $\eta_k = \eta \le 0.5 \ \forall k$ has been chosen. The Newton-BiCGStab method stops if the following stopping criterion is satisfied:

$$\left\| \underline{F}(\underline{x}) \right\| < Tol\,. \tag{21}$$

The same strategy based on the Newton - BiCGStab methods (this time without preconditioner) has been used in order to solve Eq. (15). In this circumstance, due to the small dimensions of the problem, the arising linear systems can be also solved by means of direct methods. Therefore a second strategy based on this kind of procedures (the Newton – LU

methods [23]) has been analyzed and experimented on the system (15). The employment of this alternative approach needs the computation and the storage of the whole Jacobian at each nonlinear iteration. The comparison between the performances of the different strategies will be reported in following chapter.

As regards the time integration of the whole model (multibody model and contact model; see Fig. (2)), explicit ODE solvers with variable step and variable order have been considered. [24] Moreover, during the simulations, the initial conditions for the nonlinear solvers (i. e. the Newton – BiCGStab and Newton – LU methods) are continually updated in order to speed up the convergence of the solvers and to reduce the computation time. In other words the solution of the problem at the current time step is used as initial condition for the solver at the next time step.

6 NUMERICAL SIMULATIONS

In order to study the behaviour of the whole model, a large number of simulations has been carried out on many different railway tracks. The performances of the model have been evaluated both in terms of output accuracy (kinematic variables, contact forces and contact patch) and in terms of numerical efficiency (performances of the numerical algorithms and time consumption).

6.1 Performances of the numerical methods

In this section the performances of the numerical procedures described in the previous chapter will be analyzed and compared to each other. To this purpose a typical simulation of the lateral dynamics of the Manchester Wagon has been considered. [5] [17] The simulations have been performed on a curvilinear railway track, the data of which are reported in Tab. (3).

Curvature	K	$1/1200$ m^{-1}
Slope	p	0
Cant	β	60 mm
Laying angle	α_p	$1/40$ rad
Velocity	V	45 m/s
Friction coefficient	μ	0.3

Table 3: Data of the railway track.

Differential Contact Model	Eq. (12)	Eq. (15)
RelTol / AbsTol	$10^{-8}/10^{-6}$	$10^{-8}/10^{-6}$
Nonlinear Solver	Newton - BiCGStab	Newton - BiCGStab
Tol / MaxitNonlin	$10^{0}/20$	$10^{-8}/20$
η / MaxitLin	0.01 / 20	0.01 / 20

Table 4: Numerical parameters.

The comparison between the numerical methods has been carried out on a machine equipped with an Intel Xeon 2.66GHz, 8GB RAM using Matlab R2007b (machine precision $\varepsilon_m = 2*10^{-16}$).

In order to compare the contact problem formulations (12) and (15) and to establish the best ODE solver, several experimentations have been performed with the ODE23 and the ODE45. [24] The value of the main numerical parameters are reported in Tab. (4) for both the formulations. RelTol and AbsTol are the relative and absolute tolerances of the ODE solvers, MaxitNonlin, MaxitLin are the maximum number of nonlinear and linear iterations, Tol is the stopping tolerance and η is the forcing term. In particular the values of the stopping tolerance Tol have been chosen to assure a sufficient accuracy (in terms of displacements and contact pressures) and, at the same time, to minimize the computation time.

Tab. (5) summarizes the results obtained by using the ODE 23 and relative respectively to formulation (12) (large and sparse systems) and to formulation (15) (small and full systems). Similarly Tab. (6) reports the same results obtained by using the ODE 45. For each wheel – rail contact pair (Left and Right) the following data have been considered: the number #cps of contact problem solved (equal for both the contact pairs), the total number #New of nonlinear iterations, the average number #BiCGS of linear iterations for each nonlinear iteration and the total computation time.

Differential Contact Model: Eq. (12)				
	#cps	#New	#BiCGS	time
R	29435	31390	4.3	31236
L		32610	4.6	8h 40min

Differential Contact Model: Eq. (15)				
	#cps	*#New*	#BiCGS	time
R	31814	27409	2.9	8396
L		29495	3.5	2h 20min

Table 5: Comparison between the formulation (12) and (15) using the ODE23.

Differential Contact Model: Eq. (12)				
	#cps	#New	#BiCGS	time
R	38365	49126	5.6	48753
L		51399	4.7	13h32min

Differential Contact Model: Eq. (15)				
	#cps	*#New*	#BiCGS	time
R	45710	44625	3.1	12870
L		46170	3.5	3h 34min

Table 6: Comparison between the formulation (12) and (15) using the ODE45.

The results show that the formulation (15) is more efficient than formulation (12) even though the solution of Eq. (15) requires a bigger memory consumption. Moreover in both cases low order solvers like the ODE23 turn out to be better than high order solvers like ODE45.

As said in the paragraph 5.5, Eq. (15) can be also solved by means of a Newton – LU strategy. Tab (7) contains the results obtained by comparing the Newton – LU and the Newton – BiCGStab methods. The used ODE solver is the ODE23 while the other numerical parameters are the same reported in Tab. (4).

Nonlinear solver: Newton - LU			
	#cps	#New	time
R	30401	23936	39096
L		24306	10h 51min

Nonlinear solver: Newton - BiCGStab				
	#cps	#New	#BiCGS	time
R	31814	27409	2.9	8396
L		29495	3.5	2h 20min

Table 7: Comparison between the Newton – LU and the Newton – BiCGStab methods.

Looking at Tab. (7), the Newton – BiCGStab methods (matrix free) are more efficient than the Newton – LU methods. In particular the computation and the storage of the Jacobian matrix at each nonlinear iteration turned out to be too time-consuming.

Finally, in order to justify the choice of the constant forcing term $\eta = 10^{-2}$, some experimentations have been performed by using the following values of the parameter: $\eta = 0.5,\ 10^{-1},\ 10^{-2},\ 10^{-3},\ 10^{-4}$. As usual the formulation (15) has been considered while

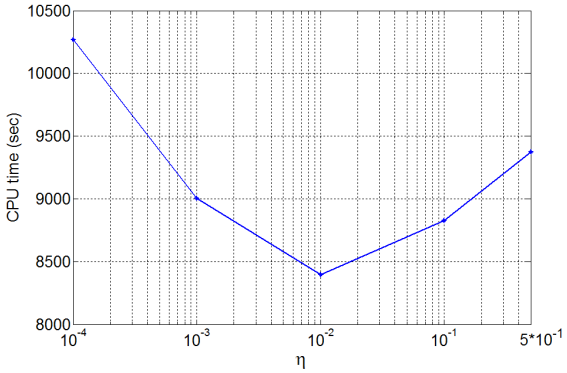

Figure 9: Computation time as a function of the forcing term η.

the employed ODE solver is always the ODE23. The results have been reported in terms of computation time (see Fig.(9)).

6.2 The SIMPACK RAIL 2D multibody model

The same multibody model of the benchmark vehicle (the Manchester Wagon [16]) has been implemented also in Simpack Rail, a widely tested and validated multibody software for the analysis of the railway vehicle dynamics. This time the multibody model is equipped with a standard contact model based on the semi – elastic approach. [4] [5] [6] As in the previous case the 2D multibody model (designed for the study of the lateral dynamics) has been obtained from the fully 3D multibody model of the vehicle while the contact model is completely 3D (see Fig. (10)).

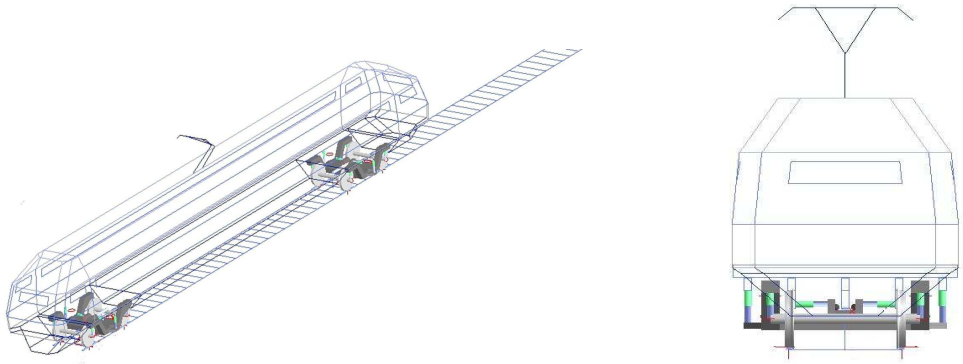

Figure 10: 3D and 2D multibody models of the Manchester Wagon (Simpack Rail).

The comparison between the results obtained by the Matlab/Simulink model and those obtained by the Simpack Rail model has allowed an accurate and reliable validation of the new contact model.

6.3 Simulation of the lateral vehicle dynamics

The comparison between the Matlab/Simulink model (implemented on Matlab R2007b) and the Simpack Rail model (implemented on Simpack 8.900) has been carried out on the same curvilinear railway track introduced above (see Tab. (3)). [5] [17] The numerical data relative to the Matlab model have been chosen starting from the results obtained in the paragraph 6.1 (Tab. (8)). Similarly the numerical data relative to the Simpack model are briefly summarized in Tab. (9).

ODE Solver	ODE 23 (Bogacki - Shampine)
RelTol / AbsTol	10^{-8} / 10^{-6}
Contact Model	Differential Contact Model: Eq. (15)
Nonlinear Solver	Newton - BiCGStab
Tol / MaxitNonlin	10^{-8} / 20
η / MaxitLin	0.01 / 20

Table 8: Numerical Data (Matlab model).

ODE Solver	ODE 5 (Dormand - Prince)
Fixed Step	$5*10^{-4}$
Contact Model	Semi – Elastic Approach

Table 9: Numerical Data (Simpack model).

Among all the kinematic and dynamic variables evaluated by the models, the time histories of the following quantities are reported (for the sake of simplicity all the outputs are expressed in the reference system $O_R x_R y_R z_R$):

- the lateral displacement y_W^R of the centre of mass of the wheelset $\underline{O}_W^R$ (Fig. (11))
- the lateral displacement y_B^R of the centre of mass of the body – car $\underline{O}_B^R$ (Fig. (12))
- the contact forces on the left wheel $\underline{F}_{lw}^R$ and on the right wheel $\underline{F}_{rw}^R$; in particular Y_{lw}^R and Y_{rw}^R are the lateral forces (Fig. (13) and Fig. (15)) while Q_{lw}^R and Q_{rw}^R are the vertical forces (Fig. (14) and Fig. (16)).

The Matlab variables are plotted in blue while the equivalent Simpack quantities in red.

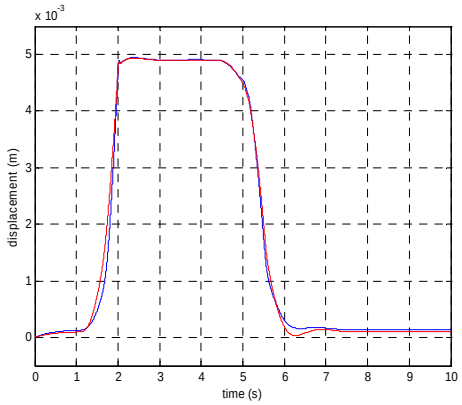

Figure 11: Lateral displacement y_W^R

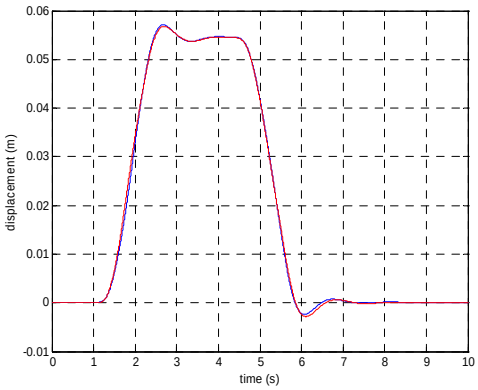

Figure 12: Lateral displacement y_B^R

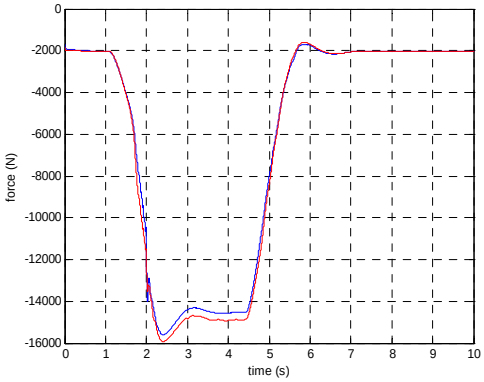

Figure 13: Lateral force Y_{lw}^R

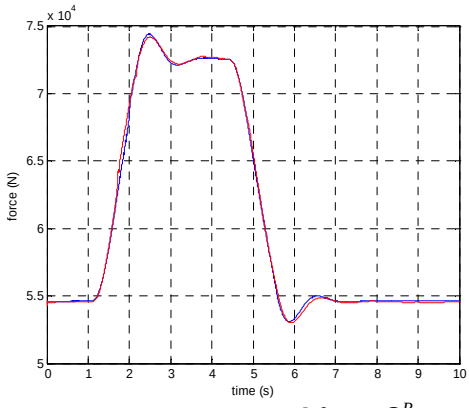

Figure 14: Vertical force Q_{lw}^R

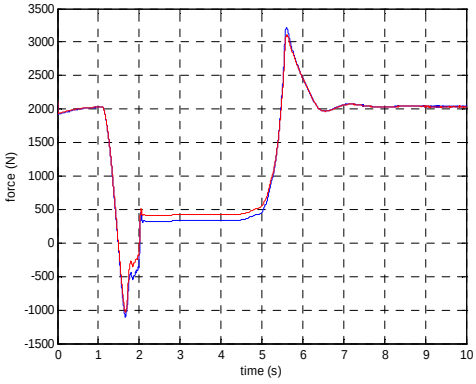

Figure 15: Lateral force Y_{rw}^R

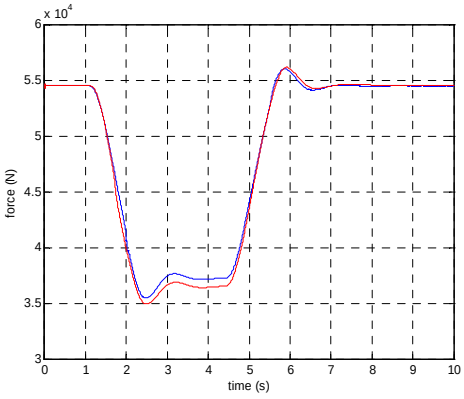

Figure 16: Vertical force Q_{rw}^R

The simulation results show a good agreement between the Matlab model and the Simpack model both in terms of kinematic variables and in terms of contact forces.

As regards the positions of contact patches A_{wC}, A_{rC} on the wheel and on the rail, in order to give an effective description of the shifting of the contact areas during the simulation, a lateral section along the plane $y_R z_R$ of the areas A_{wC}, A_{rC} has been considered. Moreover the sections of the contact patches have been plotted on cylindrical surfaces generated by the wheel and rail profiles and as long as the distance traveled by the vehicle. By convention A_{lwC}, A_{rwC} are the contact areas on the left and on the right wheel (Fig. (17) and Fig. (18)) while A_{lrC}, A_{rrC} are the contact areas on the left and on the right rail (Fig. (19) and Fig. (20)).

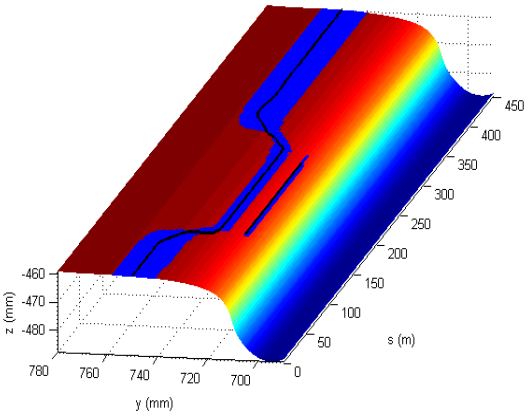

Figure 17: Section of contact area A_{lwC}

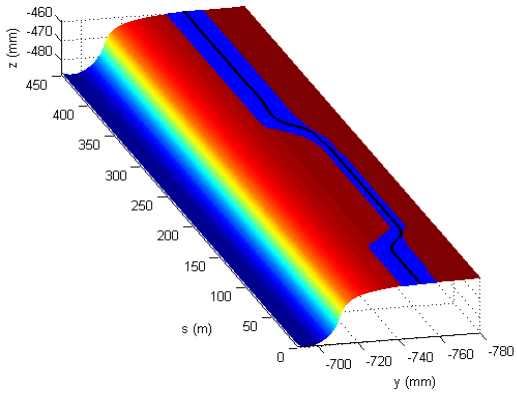

Figure 18: Section of contact area A_{rwC}

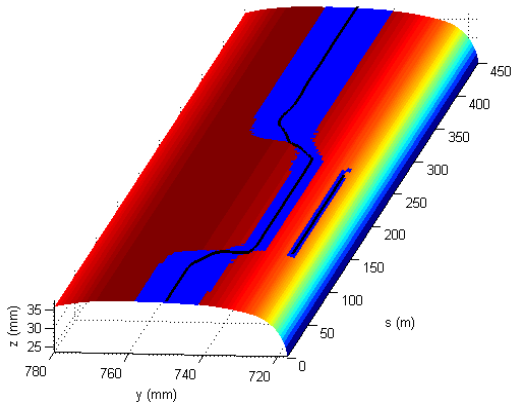

Figure 19: Section of contact area A_{lrC}

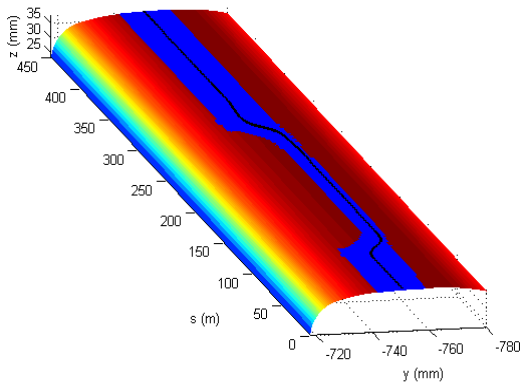

Figure 20: Section of contact area A_{rrC}

The sections of the contact areas evaluated by the Matlab model are plotted in blue while the contact points detected by the Simpack model are plotted in black. It is interesting to remark that, during the curve, a second contact point appears on the left wheel and rail (the track turns to left). Consequently, while the Simpack model detects two distinct contact points, the contact areas evaluated by the Matlab model consist of two disjoint parts. Also in this case the agreement between the results obtained by the Matlab model and the Simpack model is good.

In conclusion the accuracy of the Matlab model turns out to be comparable with that of the Simpack model; moreover the quasi – total absence of numerical noise highlights the robustness and the stability of the new differential contact model.

7 CONCLUSIONS AND FURTHER DEVELOPMENTS

The performances of the Matlab model turned out to be good both in terms of output accuracy (kinematic variables, contact forces and contact patch) and in terms of numerical efficiency (performances of the numerical algorithms and time consumption) and satisfy all the specifics reported in the introduction (see chapter 1).

As regards the further developments, in the near future fully 3D multibody models of the Manchester Wagon will be considered. This kind of model allows a complete description of the vehicle dynamics but obviously involves an increase of the model DOFs and of the number of wheel – rail contact pairs.

Moreover many optimizations of the differential contact model are planned for the future. The improvements will regard especially the FEM techniques used to discretize the contact problem. In particular new mesh generation algorithms and suitable nonlinear shape functions will be examined. These techniques assure a better accuracy in the description of the local contact phenomena but increases the dimension of the discrete problem and consequently the computational load and the memory consumption.

Finally the implementation of the contact model in programming environments like C/C++ and FORTRAN will be considered in order to obtain a further reduction of the computation time.

ACKNOWLEDGEMENTS

The authors would like to thank S. Bellavia and B. Morini of the Section of Numerical Analysis of the Energy Engineering Department (University of Florence) for the valuable suggestions provided during the development and the implementation of the numerical procedures.

REFERENCES

[1] A. A. Shabana, J. R. Sany. An augmented formulation for mechanical systems with non-generalized coordinates: application to rigid body contact problems. *Nonlinear Dynamics*, **24**, 183 – 204, 2001.

[2] S. Iwinicki. Simulation of wheel – rail contact forces. *Fatigue and Fracture of Engineering Materials and Structures*, **26**, 887 – 900, 2003.

[3] J. Pombo, J. Ambrosio. Dynamic analysis of a railway vehicle in real operation conditions using a new wheel – rail contact detection model. *International Journal of Vehicle Systems Modelling and Testing*, **1**, 79 – 105, 2005.

[4] J. J. Kalker. *Three – dimensional Elastic Bodies in Rolling Contact*. Kluwer Academic Publishers, Dordrecht, Netherlands, 1990.

[5] R. V. Dukkipati, J. R. Amyot. *Computer Aided Simulation in Railway Dynamics*. Dekker, New York, 1988.

[6] O. Polach. Creep forces in simulations of traction vehicles running on adhesion limit. *Wear*, **258**, 992 – 1000, 2005.

[7] A. A. Shabana, K. E. Zaazaa, J. L. Escalona, J. L. Sany. Development of elastic force model for wheel/rail contact problems. *Journal of Sound and Vibration*, **269**, 295 – 325, 2004.

[8] J. Auciello, M. Malvezzi, E. Meli, A. Rindi. Comparison between two multibody codes for the simulation of the railway vehicle dynamics. WCCM8 - ECCOMAS 2008, Venice, Italy, June 30 – July 4, 2008.

[9] S. Falomi, M. Malvezzi, E. Meli, A. Rindi. Determination of wheel – rail contact points with semianalytic methods. *Multibody System Dynamics*, **20**, 4, 327 – 358, 2008.

[10] G. Duvaut, J. L. Lions. *Les Inequations en Mecanique et en Physique*. Dunod, Paris, France, 1972.

[11] K. L. Johnson. *Contact Mechanics*. Cambridge University Press, Cambridge, England, 1985

[12] N. Kikuchi, J. T. Oden. *Contact Problems in Elasticity*. SIAM Studies in Applied Mathematics, Philadelphia, Pennsylvania, 1988.

[13] P. Wriggers. *Computational Contact Mechanics*. John Wiley & Sons, Hoboken, New Jersey, 2002.

[14] O. Zienkiewicz. *The Finite Element Method in Engineering Science*. McGraw – Hill, New York, 1988.

[15] A. Klarbring. A mathematical programming approach to 3D contact problems with frictions. *Computer Methods in Applied Mechanics and Engineering*, **58**, 175 – 200, 1986.

[16] S. Iwinicki. *The Manchester Benchmarks for Rail Vehicle Simulators*. Swets & Zeitlinger, Lisse, Netherlands, 1999.

[17] C. Esveld. *Modern Railway Track*. Delft University of Technology, Delft, Netherlands, 2001.

[18] G. Dhatt, G. Touzot. *The Finite Element Method Displayed*. John Wiley & Sons, Hoboken, New Jersey, 1984.

[19] G. Vicuna. *Organizzazione e Tecnica Ferroviaria*. Ed. CIFI, Roma, Italy, 1986.

[20] R. S. Dembo, S. C. Eisenstat, and T. Steihaug. Inexact Newton methods. *SIAM Journal of Numerical Analysis*, **19**, 400 – 408, 1982.

[21] C.T. Kelley. *Iterative Methods for Linear and Nonlinear Equations*. SIAM, Philadelphia, Pennsylvania, 1995.

[22] Y. Saad. *Iterative Methods for Sparse Linear Systems*. SIAM, Philadelphia, Pennsylvania, 2003.

[23] J. Nocedal, S.J. Wright. *Numerical Optimization*. Springer Series in Operation Research, Berlin, Germany, 1999.

[24] L. F. Shampine, M. W. Reichelt. The MATLAB ODE Suite. *SIAM Journal on Scientific Computing*, **18**, 1 – 22, 1997.